



**HAL**  
open science

## Heterogeneous fenton and photo-fenton oxidation for paracetamol removal using iron containing ZSM-5 zeolite as catalyst

Filipa Aleksandrova Velichkova, Henri Delmas, Carine Julcour-Lebigue,  
Bogdana Koumanova

► **To cite this version:**

Filipa Aleksandrova Velichkova, Henri Delmas, Carine Julcour-Lebigue, Bogdana Koumanova. Heterogeneous fenton and photo-fenton oxidation for paracetamol removal using iron containing ZSM-5 zeolite as catalyst. *AICHE Journal*, 2017, 63 (2), pp.669-679. 10.1002/aic.15369 . hal-02134785

**HAL Id: hal-02134785**

**<https://hal.science/hal-02134785>**

Submitted on 20 May 2019

**HAL** is a multi-disciplinary open access archive for the deposit and dissemination of scientific research documents, whether they are published or not. The documents may come from teaching and research institutions in France or abroad, or from public or private research centers.

L'archive ouverte pluridisciplinaire **HAL**, est destinée au dépôt et à la diffusion de documents scientifiques de niveau recherche, publiés ou non, émanant des établissements d'enseignement et de recherche français ou étrangers, des laboratoires publics ou privés.



## Open Archive Toulouse Archive Ouverte (OATAO)

OATAO is an open access repository that collects the work of some Toulouse researchers and makes it freely available over the web where possible.

This is an author's version published in: <http://oatao.univ-toulouse.fr/20832>

**Official URL:** <https://doi.org/10.1002/aic.15369>

### To cite this version:

Velichkova, Filipa Aleksandrova and Delmas, Henri and Julcour-Lebigue, Carine and Koumanova, Bogdana Heterogeneous fenton and photo-fenton oxidation for paracetamol removal using iron containing ZSM-5 zeolite as catalyst. (2016) *AIChE Journal*, 63 (2). 669-679. ISSN 0001-1541

Any correspondence concerning this service should be sent to the repository administrator:

[tech-oatao@listes-diff.inp-toulouse.fr](mailto:tech-oatao@listes-diff.inp-toulouse.fr)

# Heterogeneous Fenton and Photo-Fenton Oxidation for Paracetamol Removal Using Iron Containing ZSM-5 Zeolite as Catalyst

**Filipa Velichkova**

Laboratoire de Génie Chimique, Université de Toulouse, CNRS, INPT, UPS, Toulouse, France  
Dept. of Chemical Engineering, University of Chemical Technology and Metallurgy, 8 Kliment Ohridsky Blvd.,  
1756 Sofia, Bulgaria

**Henri Delmas and Carine Julcour**

Laboratoire de Génie Chimique, Université de Toulouse, CNRS, INPT, UPS, Toulouse, France

**Bogdana Koumanova**

Dept. of Chemical Engineering, University of Chemical Technology and Metallurgy, 8 Kliment Ohridsky Blvd.,  
1756 Sofia, Bulgaria

DOI 10.1002/aic.15369

*Paracetamol is commonly found in wastewaters, as a consequence of its high consumption and incomplete elimination by conventional treatments. Homogenous (photo-)Fenton oxidation has proved efficient for its remediation, but it suffers from uneasy dissolved iron recovery. Therefore this work examines the performance and stability of an iron containing zeolite (Fe/MFI) as catalyst for this reaction. Effects of reaction parameters (pH, temperature, catalyst and H<sub>2</sub>O<sub>2</sub> concentrations, UV/vis irradiation) are investigated in batch conditions, by comparing the pollutant and Total Organic Carbon disappearance rates in solution, as well as the overall mineralization yield (including solid phase) and oxidant consumption. At near neutral pH paracetamol can be fully converted after 5 h, while TOC removal reaches up to 60%. Finally, thanks to good catalyst stability (low leaching), a continuous process coupling oxidation and membrane filtration is proposed, showing constant TOC conversion over 40 h and iron loss in the permeate <0.3 ppm. c*

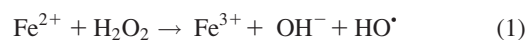
*Keywords: water, advanced oxidation, Fenton-like, catalytic processes, immobilization*

## Introduction

Water quality in the natural environment, and hence supply of drinking water is one of the great issues of our industrialized societies. Among the emergent pollutants, pharmaceuticals have become one of the main targets in addition to pesticides and other persistent organic pollutants (POPs). For instance, in Europe, about 4000 different pharmaceutical compounds are susceptible to be released in the environment.<sup>1</sup> Although long-term effects and minimal effect concentrations are still subject of controversy, data available to date clearly indicate that some pharmaceutical compounds develop multi-resistant strains in microorganisms, can be noxious for algae and invertebrates and affect the endocrine system of fishes.<sup>2</sup> One of the main reasons for the occurrence of these effects is that pharmaceuticals are designed to have a complex structure,

and most of the conventional treatments are not able to eliminate them, or at least to transform them into more benign products. Hence more powerful and specific treatment processes are to be developed to deal with this new pollution.

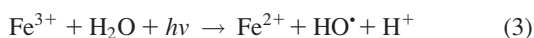
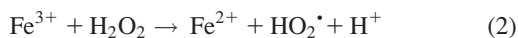
Advanced oxidation processes (AOPs) have proved to be efficient for the elimination of pharmaceuticals from water, either in replacement or complement of biological treatments.<sup>3</sup> They are based on the production of highly reactive species, primarily the nonselective hydroxyl radicals (HO<sup>•</sup>) able to oxidize most of the organic molecules, yielding short-chain organic acids, CO<sub>2</sub>, H<sub>2</sub>O, and inorganic ions as end-products. Of these, Fenton oxidation uses the decomposition of hydrogen peroxide with dissolved ferrous salt as a catalyst to generate HO<sup>•</sup> involving a complex reaction sequence, starting with:



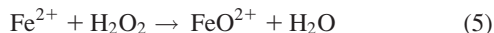
Regeneration of ferrous iron (Eq. 2) is recognized as the limiting step of this catalytic process, but its rate can be enhanced by UV/vis irradiation providing additional radicals, according to Eqs. 3 (photo-reduction of Fe<sup>3+</sup>) and 4 (photolysis of H<sub>2</sub>O<sub>2</sub>).<sup>4</sup>

---

Correspondence concerning this article should be addressed to C. Julcour at carine.julcour@ensiacet.fr.



A nonradical mechanism has been also reported,<sup>4,5</sup> involving the formation of ferryl ion, an oxidizing  $\text{Fe}^{\text{IV}}$  species:



The main drawback of this homogeneous process comes from the necessity of a posttreatment, as usual iron concentrations of tens of ppm are much higher than the maximum discharge concentration (2 ppm in EU<sup>6</sup>). Moreover Fenton oxidation operates within a narrow pH range, usually between 2 and 4, mostly to prevent iron precipitation during the reaction. Neutralization of the effluent usually follows the oxidation process both to remove iron and reach the release standards, producing hardly disposable sludge, besides chemical consumption and catalyst lost.

To overcome these drawbacks, heterogeneous iron-based catalysts have been used in the so-called Fenton-like process, allowing wider operated pH ranges and facilitating the reuse of catalyst.<sup>7–13</sup>

Fe-containing zeolites are interesting candidates as heterogeneous Fenton catalyst because of the combination of their adsorptive and catalytic properties. They have shown high catalytic activity in the oxidation of organic compounds, with minimal iron leaching.<sup>14–18</sup> Considering the removal of pharmaceutical compounds, until now such materials have been mainly investigated as adsorbents.<sup>19,20</sup>

The purpose of this work is to investigate the catalytic activity of a commercial Fe-containing zeolite of ZSM-5 type in the Fenton and photo-Fenton oxidation of paracetamol. Paracetamol is one of the most commonly used painkiller in the world, and consequently it is detected in urban wastewater treatment plants and in many environment compartments.<sup>21–24</sup> Several works have been reported on its degradation by (photo-)Fenton process, but essentially carried out with homogeneous systems.<sup>25–29</sup> In this study, the influence of different operating conditions—pH, temperature, catalyst concentration, oxidant concentration, and UV irradiation—is evaluated for the heterogeneous reaction. As most of the works dedicated to the degradation of paracetamol by AOPs<sup>25–32</sup> used concentration levels as high as 1 mmol L<sup>-1</sup>, the initial pollutant concentration was set to 100 ppm for comparison purpose. Moreover, for very diluted effluents, AOPs would probably be better used downstream a pre-concentration step so as to treat smaller streams, limit radical scavenging and save chemicals.<sup>33</sup> This also allows both the liquid and the solid phases to be analyzed with enough precision to determine the fate of the pollutant during the batch oxidation. Iron leaching and catalyst stability are also considered. Finally a proof of concept of the continuous treatment process coupling heterogeneous photo-Fenton oxidation and membrane filtration is presented.

## Materials and Methods

### Chemicals and catalysts

Paracetamol (N-(4-hydroxyphenyl)acetamide) was supplied by BioXtra with a purity  $\geq 99.0\%$ . Hydrogen peroxide (Ph Eur, 30% w/w, Sigma-Aldrich) and a commercial iron-containing zeolite of ZSM-5 structure (Fe-MFI-27, labeled as “Fe/MFI”, provided by Süd-Chemie AG) were used as Fenton’s reagents. This zeolite exhibited a Si/Al ratio of 13 and an

iron content of 3.5 wt %. The performance of the parent zeolite (H-MFI-27, without iron and labeled as “MFI”) was also assessed.

During the Fenton and photo-Fenton experiments, samples of the reactant mixture were withdrawn at different reaction times and mixed with a quenching solution containing KI (0.1 mol L<sup>-1</sup>), Na<sub>2</sub>SO<sub>3</sub> (0.1 mol L<sup>-1</sup>), and a phosphate buffer (mixture of KH<sub>2</sub>PO<sub>4</sub>, 0.05 mol L<sup>-1</sup> and Na<sub>2</sub>HPO<sub>4</sub>·2H<sub>2</sub>O, 0.05 mol L<sup>-1</sup>; pH 7.2). KI and Na<sub>2</sub>SO<sub>3</sub> reduce H<sub>2</sub>O<sub>2</sub>, while the phosphate buffer precipitates leached iron.<sup>34</sup> All these reagents were analytical grade and supplied by Sigma-Aldrich.

### Experimental setups and protocols

Three different experimental setups have been used to investigate, respectively, the “dark” and UV-assisted Fenton oxidations in a batch mode, and the continuous photo-Fenton process. Some Fenton experiments were repeated to check for the reproducibility of concentration-time profiles of pollutant and TOC. Pooled standard deviations ( $s_p$ ) were estimated from each of the corresponding sets of duplicate concentrations:

$$s_p = \sqrt{\frac{\sum_{i=1}^k d_i^2}{2k}} \quad (6)$$

where  $k$  is the total number of data points and  $d_i$  is the difference in duplicate measurements. For paracetamol, only concentrations higher than 1 mg L<sup>-1</sup> were accounted for. The resulting error bar was  $\pm 1$  mg L<sup>-1</sup> for paracetamol and  $\pm 3$  mg L<sup>-1</sup> for TOC.

**Batch Reactors.** The experimental setup used for *Fenton oxidation* consisted in a 1 L stirred Pyrex reactor, equipped with a jacket to maintain the temperature of the suspension.

The *photo-Fenton* system (Supporting Information Figure S1A) included two-glass reactors equipped with a double jacket, connected to a cryothermostat: a photochemical reactor (comprising 0.5 L of solution) enclosed in a safety cabinet and an auxiliary reactor (1 L capacity) for sampling. The first reactor was stirred by a magnetic stirrer and the second one was equipped with baffles and a pitched-blade impeller. The suspension was fast recycled between the two reactors by means of a dual-head peristaltic pump at a flow rate of 100 mL min<sup>-1</sup> to approach a perfectly stirred behavior. Moreover air was gently bubbled into the photochemical reactor to prevent catalyst sedimentation and insure a uniform suspension concentration, as confirmed by weighing of the solid in the two reactors. The photochemical reactor was equipped with a thermostated Pyrex immersion well including a medium-pressure mercury vapor lamp (PC451.050 Hannovia lamp, 450 W, arc length 4.8 cm). The lamp emitted 176 W: 40%–48% in the ultraviolet, 40%–43% in the visible and the rest in the infrared. The Pyrex lamp holder completely cut wavelengths below 280 nm, about 50% of the emission at 310 nm and gave a transmittance of 94% above 355 nm. Paracetamol exhibiting a light absorption maximum at 245 nm, photolysis contribution was very low in these conditions.

100 mg L<sup>-1</sup> (0.66 mmol L<sup>-1</sup>) paracetamol solutions prepared with osmosed water were used. Agitation speed was set to 350 rpm. For some experiments, the initial pH of the solution was adjusted to 2.8 with H<sub>2</sub>SO<sub>4</sub> 10%, after which the catalyst powder was added. A sequential procedure was performed in all cases: the suspension was first stirred during 180 min to approach the adsorption equilibrium, as confirmed by the

chromatography analysis of samples withdrawn at different times. Then, oxidation was initiated by adding H<sub>2</sub>O<sub>2</sub>. For photo-Fenton experiments, the UV lamp was turned on 10 min before oxidant addition to reach full output prior to oxidation starting. It was checked that photolysis was negligible during this preliminary period.

**Continuous Treatment System.** It included the same photochemical reactor, but a larger auxiliary reactor (about 2.5 L capacity) equipped with an immersed microfiltration membrane to retain the dispersed catalyst within the system (Supporting Information Figure S1B). This membrane was placed on the suction line of an additional dual-head peristaltic pump that also fed the reactor with an aqueous solution of paracetamol (100 mg L<sup>-1</sup>) and H<sub>2</sub>O<sub>2</sub> (28 mmol L<sup>-1</sup>), maintaining a constant liquid level. The filtration module (provided by Polymem<sup>TM</sup>) consisted in U-shaped assembly of polysulfone hollow fibers with a nominal pore size of 0.1 μm and a total filtering surface of 0.1 m<sup>2</sup>. The reaction was started by addition of the catalyst into the membrane reactor (filled with the paracetamol and H<sub>2</sub>O<sub>2</sub> solution) and the lamp was switched on 30 min later to let time for the suspension concentration to be equilibrated in between the two reactors.

### Analytical methods

**Analysis of Aqueous Solution Samples.** Suspension samples (8 mL) were periodically taken and first filtered on a nylon membrane with 0.2 μm pore size.

The evolution of *paracetamol concentration* was monitored by a high performance liquid phase chromatograph (HPLC) equipped with a diode array detector (UV6000, Thermo Finnigan). The stationary phase consisted in a C18 reverse phase column (ProntoSIL C18 AQ) and the mobile phase (10/90 mixture of acetonitrile and deionized water acidified at pH 2.0 with H<sub>3</sub>PO<sub>4</sub>) was fed at 1 mL min<sup>-1</sup> using isocratic elution. The wavelength was set to 254 nm for paracetamol detection. Quantification was made from a calibration curve periodically updated with fresh standard solutions, the relative error being less than 2%. To prevent any further oxidation in the presence of leached iron, a phosphate buffer (0.6 mL) was added to the solution (1 mL) and the mixture was again filtered before being readily injected into the chromatograph.

**Residual TOC** was also measured to evaluate mineralization of the pollutant. Prior to this analysis, 5 mL of the reacting solution were treated with 2 mL of a quenching solution (KI, 0.1 mol L<sup>-1</sup>; Na<sub>2</sub>SO<sub>3</sub>, 0.1 mol L<sup>-1</sup>; KH<sub>2</sub>PO<sub>4</sub>, 0.05 mol L<sup>-1</sup>; Na<sub>2</sub>HPO<sub>4</sub>·2H<sub>2</sub>O, 0.05 mol L<sup>-1</sup>) that reduced the remaining oxidant and precipitated dissolved iron. The sample was again filtered and diluted with ultrapure water to 24 mL. The TOC concentration was calculated from the difference between Total Carbon and Inorganic Carbon concentrations measured with a Shimadzu TOC-V<sub>CSN</sub> analyzer. Quantification limit for TC was 0.5 mg L<sup>-1</sup>. Reported values corresponded to the mean of three successive measurements showing a coefficient of variation (CV) of less than 2%. Identification of reaction intermediates was performed during a Fenton oxidation test by HPLC/MS/UV: acetamide was identified as the main by-product (with a concentration up to 0.35 mmol L<sup>-1</sup>), followed by carboxylic acids (among them mainly glycolic and oxamic acids, when excluding formic acid also present in the eluent). Toxic intermediates such as hydroquinone and *p*-benzoquinone were either found in a very low amount (less than 0.005 mmol L<sup>-1</sup>) or not detected. Other intermediates bearing a nitrogen group were also observed (C<sub>7</sub>H<sub>7</sub>O<sub>2</sub>N, C<sub>6</sub>H<sub>7</sub>O<sub>5</sub>N, C<sub>16</sub>H<sub>16</sub>O<sub>4</sub>N<sub>2</sub>, and three forms of C<sub>8</sub>H<sub>9</sub>O<sub>3</sub>N), but apparently in

a trace amount (no available standard). However carbon balance could not be satisfied with respect to residual TOC.

**Residual H<sub>2</sub>O<sub>2</sub> concentration** was determined at the end of the experiments by titration with a 0.02 mol L<sup>-1</sup> permanganate solution (standardized with sodium oxalate prior to use). The coefficient of variation (CV) of the triplicate measurements was always less than 5%.

**Leached iron** in the final solution was measured by Inductively Coupled Plasma Atomic Emission Spectroscopy (Ultima 2, Horiba Jobin-Yvon), after filtration through a 0.2 μm cellulose acetate membrane. Limit of quantification was 10 μg L<sup>-1</sup>.

**Characterization of the Catalysts.** The fresh zeolites were characterized by gas porosimetry, SEM and granulometry for morphological and textural properties, as well as by XRD, Mössbauer spectroscopy, TEM/EDX and CO chemisorption to determine the nature and dispersion of the iron deposit on the zeolitic structure.

Brunauer–Emmett–Teller (BET) surface area and porous volume of the powdered catalysts were measured using nitrogen adsorption on a Micromeritics ASAP 2010 instrument. The solids were degassed 2 h at 60°C prior to the measurement. SEM images were obtained on a Hitachi TM3000 microscope. Particle-size distribution (PSD) was analyzed by laser diffraction on a Mastersizer 2000 apparatus (Malvern Instruments) using a Hydro 2000S wet dispersion unit with a pump rate of 1750 rpm. The refractive index and absorption coefficient were 1.503 and 0.1, respectively.

X-ray diffraction (XRD) patterns were collected on a theta/theta powder X-ray diffraction system (X'Pert PRO MPD, PANalytical Company) equipped with a fast X'Celerator detector. The diffractograms were recorded over a 2θ range of 5°–70° with a step of 0.017°. Room temperature (RT) <sup>57</sup>Fe Mössbauer spectrum of iron containing zeolite was obtained using a WissEl spectrometer. Following the results of this analysis (§ Catalyst properties), carbon monoxide chemisorption was also performed on Fe/MFI to obtain the iron crystallite size, using a Micromeritics ASAP 2010 C apparatus. Note that caution must be taken on the interpretation of such measurement for Fe/zeolite, as Fe<sup>2+</sup> ions (resulting from the preliminary reduction of ionic iron species) also chemisorb CO.<sup>35</sup> Powder sample (0.5 g) was preliminary degassed at 200°C then 400°C for 30 min and 1 h, respectively. Then the catalyst was reduced under H<sub>2</sub> flow at 450°C for 12 h (temperature ramp of 5°C min<sup>-1</sup>), evacuated 1 h at 400°C before cooling at 35°C for CO adsorption. A first isotherm was measured, then the sample was evacuated at 35°C to remove physisorbed CO and a second isotherm was recorded. The difference between the two isotherms gave chemisorbed gas amount. Finally the sample was degassed and reoxidized at 450°C under O<sub>2</sub> flow to determine the reduction efficiency.

Using a CO uptake per Fe atom of 1/2, iron dispersion D (%) was calculated from<sup>36</sup>:

$$D = \frac{1.117 \cdot X}{W \cdot f} \quad (7)$$

with *X* the chemisorbed CO amount (μmol g<sup>-1</sup>), *W* the overall iron weight percentage, *f* the reduced iron fraction measured from O<sub>2</sub> titration. Assuming uniform size and spherical shape, crystallite diameter was calculated according to:

$$d_c = \frac{96}{D} \quad (d_c \text{ in nm and } D \text{ in } \%) \quad (8)$$

TEM observation of the particles was also made on slices obtained by ultramicrotomy after resin inclusion using a JEOL

**Table 1. Physicochemical Properties of Fe/MFI and MFI**

Label	$S_{\text{BET}}$ ( $\text{m}^2 \text{g}^{-1}$ ) <sup>a</sup>	$V_{\text{meso}}$ ( $\text{cm}^3 \text{g}^{-1}$ ) <sup>a</sup>	$V_{\text{micro}}$ ( $\text{cm}^3 \text{g}^{-1}$ ) <sup>a</sup>	$V_{\text{total}}$ ( $\text{cm}^3 \text{g}^{-1}$ ) <sup>a</sup>	$d_{43}$ ( $\mu\text{m}$ ) <sup>b</sup>	%C <sup>c</sup>	%Fe <sup>d</sup>	$d_c$ (Fe) (nm) <sup>e</sup>	$\text{pH}_{\text{PZC}}$ <sup>f</sup>
Fe/MFI	329	0.05	0.13	0.18	7.9	0.02	3.4 (3.6)	4	2.8
MFI	377	0.04	0.15	0.19	21.9	0.03	–	–	4.3

<sup>a</sup>Specific surface area, mesoporous (Barrett-Joyner-Halenda method), microporous (Horváth-Kawazoe method) and total porous ( $p/p_0$  value = 0.99) volumes, measured by  $\text{N}_2$  porosimetry.

<sup>b</sup>Volume mean diameter of particles in solution from laser diffraction measurement.

<sup>c</sup>Carbon content from sample combustion and analysis of emitted  $\text{CO}_2$ .

<sup>d</sup>Iron content estimated from ICP-AES analysis of acid leachate (in brackets, value calculated from  $\text{Fe}_2\text{O}_3$  percentage given by the supplier).

<sup>e</sup>Mean diameter of iron crystallites calculated from CO chemisorption assuming a Fe:CO stoichiometry of 2:1.

<sup>f</sup>pH at the point of zero charge measured by mass titration.<sup>37</sup>

Jsm 2100F (200 kV) equipped with a SDD Bruker EDX detector for elemental analysis.

Carbon content of the zeolites (in wt %) was determined after paracetamol adsorption ( $\%C_{\text{AD}}^{\text{S}}$ ) and at the end of each oxidation ( $\%C_{\text{OX}}^{\text{S}}$ ) to estimate the overall mineralization yield of the pollutant from:

$$X_{\text{TOC}} (\%) = \frac{(\text{TOC}_{\text{AD}}^{\text{L}} - \text{TOC}_{\text{OX}}^{\text{L}}) + (\%C_{\text{AD}}^{\text{S}} - \%C_{\text{OX}}^{\text{S}}) \times \frac{[\text{zeolite}]}{100}}{\text{TOC}_{\text{AD}}^{\text{L}} + \%C_{\text{AD}}^{\text{S}} \times \frac{[\text{zeolite}]}{100}} \times 100 \quad (9)$$

where  $\text{TOC}_{\text{AD}}^{\text{L}}$  and  $\text{TOC}_{\text{OX}}^{\text{L}}$  (TOC concentration measured in the liquid phase after preliminary adsorption and at the end of oxidation, respectively) and  $[\text{zeolite}]$  are expressed in  $\text{mg L}^{-1}$ .

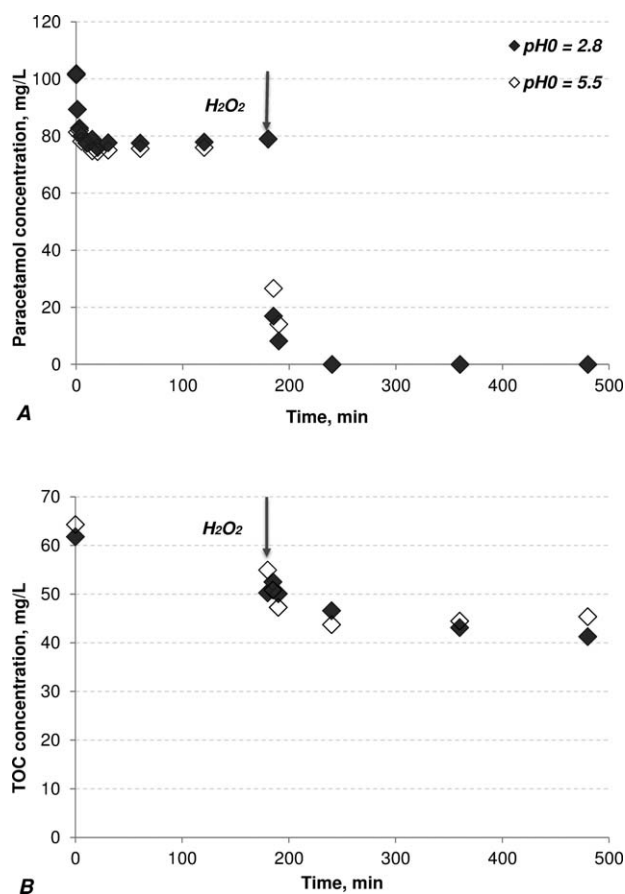


**Figure 1. Effect of pH on the wet peroxide oxidation of paracetamol on Fe/MFI: evolution of liquid phase concentrations of (A) paracetamol [P] and (B) TOC.**

Operating conditions:  $[\text{P}]_0 = 100 \text{ mg L}^{-1}$ ,  $[\text{zeolite}] = 2 \text{ g L}^{-1}$ ,  $[\text{H}_2\text{O}_2]_0 = 28 \text{ mmol L}^{-1}$ ,  $T = 60^\circ\text{C}$ .

These analyses were performed on a LECO SC144 analyzer (dosing range from 50 ppm to 10%). The sum at denominator matched with the initial TOC in solution (about  $64 \text{ mg L}^{-1}$ ) within 10%.

## Results and Discussion

### Catalyst properties

The physicochemical properties of the investigated zeolites are given in Table 1.

As expected, the zeolite powders are essentially microporous. Incorporation of 3.5% of iron reduces the microporous volume by 13%.

PSD of Fe/MFI and MFI suspension in osmosed water exhibits a main mode, centered at 4 and 10 microns, respectively, and extended from 0.5 to 30 microns. There are also a few agglomerates (less than 10% by volume) reaching several

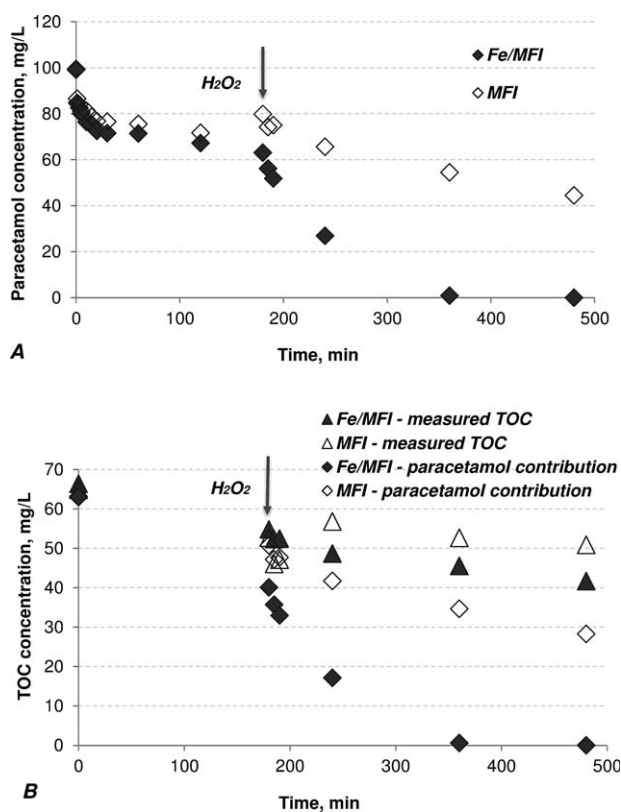
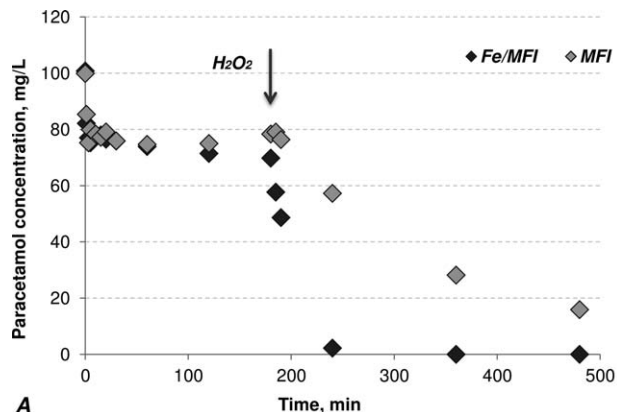
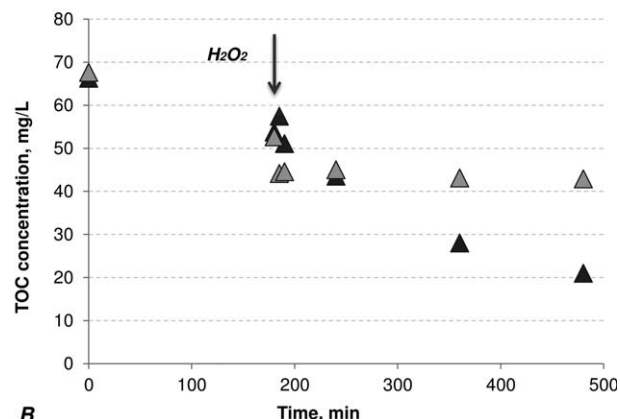


**Figure 2. Effect of iron immobilization on the zeolite catalyzed wet peroxide oxidation of paracetamol: evolution of liquid phase concentrations of (A) paracetamol and (B) TOC.**

Operating conditions:  $[\text{P}]_0 = 100 \text{ mg L}^{-1}$ ,  $[\text{zeolite}] = 2 \text{ g L}^{-1}$ ,  $[\text{H}_2\text{O}_2]_0 = 28 \text{ mmol L}^{-1}$ ,  $T = 30^\circ\text{C}$ .



A



B

**Figure 3. UV/H<sub>2</sub>O<sub>2</sub> oxidation on MFI and Fe/MFI: evolution of liquid phase concentrations of (A) paracetamol and (B) TOC.**

Operating conditions:  $[P]_0 = 100 \text{ mg L}^{-1}$ ,  $[\text{zeolite}] = 2 \text{ g L}^{-1}$ ,  $[\text{H}_2\text{O}_2]_0 = 28 \text{ mmol L}^{-1}$ ,  $T = 30^\circ\text{C}$ .

hundred microns. Corresponding volume mean diameters ( $d_{43}$ ) are given in Table 1. SEM images (not shown) confirm that the powders are rather homogeneous and formed by micronic grains.

The diffractograms of the zeolite before and after iron incorporation (Supporting Information Figure S2) were almost superimposed, and iron oxide phase corresponding to hematite (reference pattern 01-086-2368) could be hardly distinguished in the later. This could be explained by an intimate incorporation of iron into the zeolitic structure, leading to very small particles below XRD resolution. Mössbauer spectrum (Supporting Information Figure S3) exhibited the characteristic sextet of hematite at RT (isomer shift relative to metallic  $\alpha\text{-Fe}$ :  $0.37 \text{ mm s}^{-1}$ , quadrupole shift:  $-0.096 \text{ mm s}^{-1}$ , hyperfine magnetic field:  $51.5 \text{ T}$ ) and a small doublet (isomer shift:  $0.31 \text{ mm s}^{-1}$ , quadrupole splitting:  $0.79 \text{ mm s}^{-1}$ ) accounting for 7% of the spectrum area. The later could be assigned to  $\text{Fe}^{3+}$  ions in octahedral coordination.<sup>38</sup> Their contribution to CO chemisorption could be therefore neglected, which gave an iron crystallite size estimated at 4 nm. TEM/EDX also indicates the presence of a few iron-rich clusters of a few tens of nanometers (Supporting Information Figure S4).

### Preliminary considerations

*pH Effect.* The pH of the solution is one of the most important parameters in the homogeneous Fenton reaction, where optimal values range from 2 to 4. At lower values the

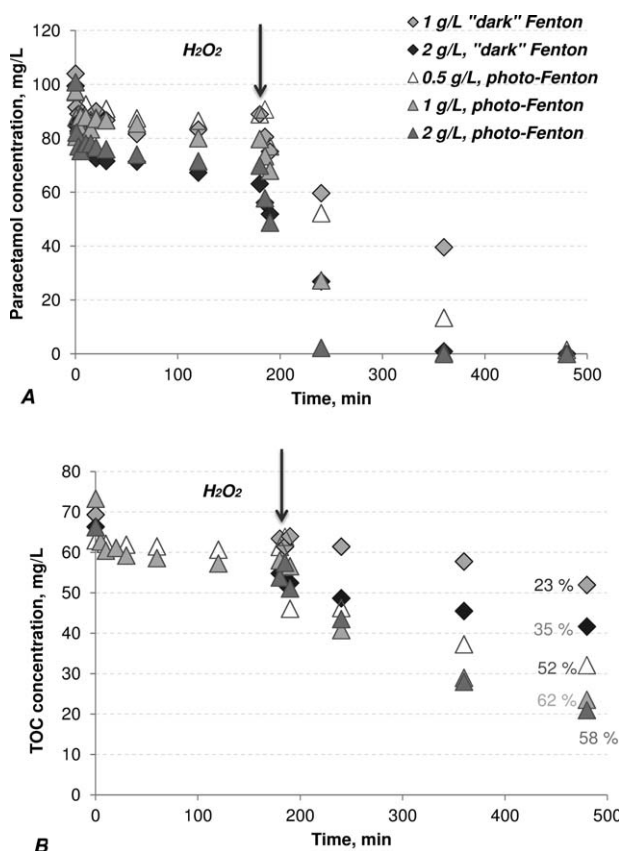
regeneration of Fe(II) is very slow, while for higher values Fe(III) precipitates into amorphous (hydr)oxides. The use of a heterogeneous catalyst system usually allows to extend the operating pH range, as immobilized Fe(II)/Fe(III) species are able to maintain an efficient redox system with  $\text{H}_2\text{O}_2$ .

To evaluate the pH effect on Fe/MFI activity, a first set of experiments was conducted at  $60^\circ\text{C}$  with and without setting the pH of the aqueous paracetamol solution at 2.8 using  $\text{H}_2\text{SO}_4$  10% (Figure 1). This temperature level was chosen as it should emphasize the pH effect by increasing the iron leaching rate. It was verified that thermal decomposition of  $\text{H}_2\text{O}_2$  at  $60^\circ\text{C}$  was negligible within the reaction time. Other conditions were as follows: Fe/MFI concentration of  $2 \text{ g L}^{-1}$  and amount of  $\text{H}_2\text{O}_2$  equivalent to two times the stoichiometric quantity required for pollutant mineralization, calculated from the following equation:



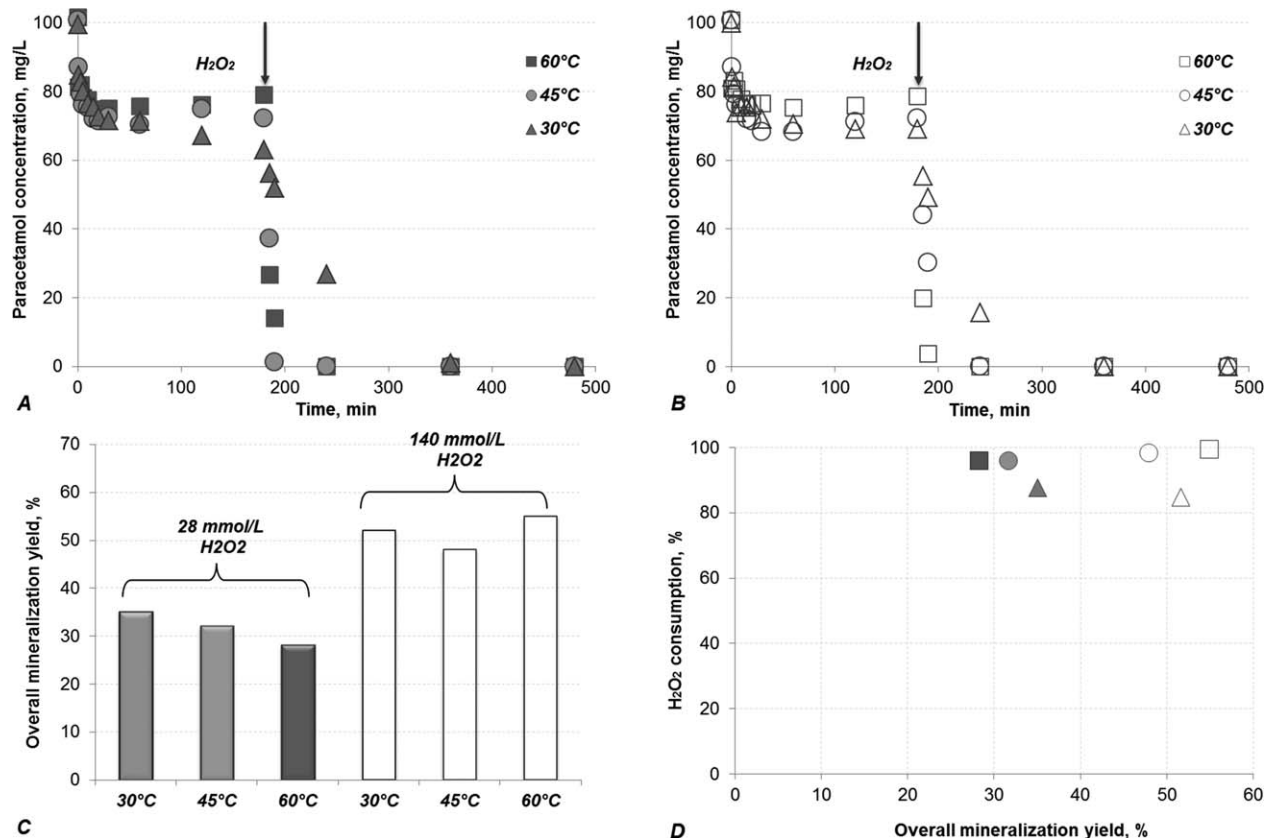
The suspension concentration was selected from preliminary adsorption isotherm measurements to insure that most of the pollutant remained in the liquid phase. Nevertheless contribution of the solid phase was also evaluated as explained above.

Figure 1A demonstrates that the adsorption equilibrium and oxidation kinetics of paracetamol are not subsequently modified by the preliminary acidification of the solution. Note that



**Figure 4. Effect of Fe/MFI concentration on "dark" Fenton and photo-Fenton oxidations: evolution of liquid phase concentrations of (A) paracetamol and (B) TOC.**

Operating conditions:  $[P]_0 = 100 \text{ mg L}^{-1}$ ,  $[\text{H}_2\text{O}_2]_0 = 28 \text{ mmol L}^{-1}$ ,  $T = 30^\circ\text{C}$ . Values in Figure 4B indicate the overall mineralization yield after 5 h of oxidation.



**Figure 5.** Effect of temperature and initial concentration of H<sub>2</sub>O<sub>2</sub> on "dark" Fenton oxidation: evolution of liquid phase concentration of paracetamol for (A) [H<sub>2</sub>O<sub>2</sub>]<sub>0</sub> = 28 mmol L<sup>-1</sup> and (B) [H<sub>2</sub>O<sub>2</sub>]<sub>0</sub> = 140 mmol L<sup>-1</sup>, (C) overall mineralization yield after 5 h of oxidation, and (D) H<sub>2</sub>O<sub>2</sub> consumption.

Operating conditions: [P]<sub>0</sub> = 100 mg L<sup>-1</sup>, [zeolite] = 2 g L<sup>-1</sup>.

the pH of the paracetamol solution decreases from 5.5 to a value close to that adjusted (3.6) by simple contact with the acidic zeolite. In this pH range—lower than the pK<sub>a</sub> value of paracetamol (9.5)—the interaction between the molecule and the surface should not be modified. The addition of H<sub>2</sub>O<sub>2</sub> led to a nearly complete elimination of paracetamol and to a moderate decrease of dissolved TOC, which as usual in "dark" Fenton conditions tended rapidly to level off (Figure 1B). Again the liquid phase concentration profiles were almost superimposed whatever the initial pH value of the solution (5.5 or 2.8). Therefore the subsequent experiments were carried out without preliminary acidification.

*Activity of the Zeolite Support with H<sub>2</sub>O<sub>2</sub> and UV/H<sub>2</sub>O<sub>2</sub>.* To estimate the separate contributions of iron deposit and zeolite support, wet peroxide oxidation was also performed on MFI. Figure 2 compares the evolution of paracetamol and TOC concentrations measured in solution with both catalysts at 30°C. In these conditions, H<sub>2</sub>O<sub>2</sub> alone did not degrade paracetamol. As expected, oxidation was clearly improved by incorporating iron into the zeolite.

Despite the loss of BET surface area, iron addition also seemed to increase paracetamol adsorption onto the zeolite, Figure 2A. TOC measured in solution after preliminary adsorption on Fe/MFI was in fact slightly higher than that calculated from paracetamol concentration only, Figure 2B, indicating a partial decomposition of the pollutant. It was confirmed by HPLC/UV analysis, which exhibited additional peaks, identified as hydroquinone and acetamide by mass

spectroscopy. This explains the apparent higher paracetamol uptake by Fe/MFI.

MFI somewhat catalyzed the wet peroxide oxidation of paracetamol, but at a much slower rate than Fe/MFI. Moreover following the adsorption stage, TOC concentration in solution remained almost unchanged after 5 h of oxidation. The small initial increase after H<sub>2</sub>O<sub>2</sub> addition might be explained by the release of less adsorbable species formed on the solid.

A complementary experiment performed without any pollutant showed that a 2 g L<sup>-1</sup> Fe/MFI suspension completely decomposed 28 mmol L<sup>-1</sup> of H<sub>2</sub>O<sub>2</sub> within 1 h at 60°C, while MFI resulted only in 25% conversion after 5 h, confirming the previous trends.

The activity of MFI was also assessed for the UV/H<sub>2</sub>O<sub>2</sub> oxidation of paracetamol on Figure 3. After 5 h of photo-oxidation on the iron-free zeolite, the pollutant was almost converted but the overall mineralization yield (accounting for carbon in both liquid and solid phases) plateaued to 21%. With Fe/MFI, both paracetamol and TOC abatement rates significantly increased, overall mineralization yield reaching 58% after 5 h.

This led to conclude that the zeolite support only slightly contributed to the catalytic activity of Fe/MFI in H<sub>2</sub>O<sub>2</sub> and UV/H<sub>2</sub>O<sub>2</sub> oxidation. All further experiments were conducted with the iron containing zeolite. As expected from Eqs. 3 to 4, comparison of concentration profiles obtained with Fe/MFI in Figure 2 and Figure 3 also indicates a clear beneficial effect of UV/vis irradiation.

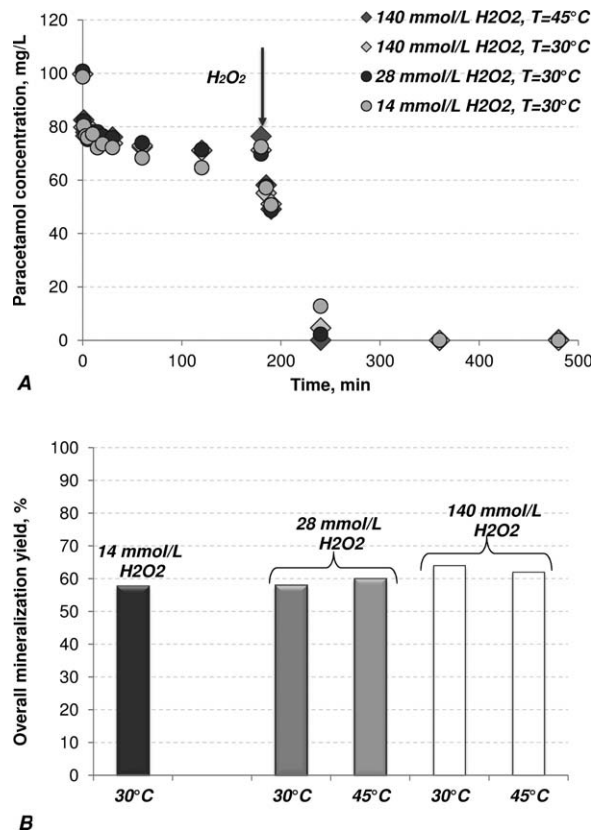


**Figure 6.** Effect of temperature and initial concentration of H<sub>2</sub>O<sub>2</sub> on photo-Fenton oxidation: (A) evolution of liquid phase concentrations of paracetamol, (B) overall mineralization yield after 5 h of oxidation.

Operating conditions:  $[P]_0 = 100 \text{ mg L}^{-1}$ ,  $[\text{zeolite}] = 2 \text{ g L}^{-1}$ .

### Parametric study of “dark” Fenton and photo-Fenton oxidation

**Catalyst Concentration.** The effect of Fe/MFI concentration is depicted on Figure 4 showing somewhat different features for “dark” Fenton and photo-Fenton oxidation.

For “dark” Fenton oxidation, increasing Fe/MFI concentration from 1 to 2 g L<sup>-1</sup> clearly improved the pollutant oxidation, as the result of increased active sites which decomposed hydrogen peroxide.

In presence of UV/vis irradiation, similar effect was observed in between 0.5 and 1 g L<sup>-1</sup> of catalyst, but it almost vanished at 2 g L<sup>-1</sup> as the overall mineralization yield was even slightly reduced, from 62% at 1 g L<sup>-1</sup> to 58% at 2 g L<sup>-1</sup>. This could be the result of reduced irradiation efficiency in more concentrated suspension due to photon absorption by the zeolite particles. This is especially true as contribution of leached iron was rather significant in photo-Fenton oxidation as shown later.

**Temperature and Initial Concentration of H<sub>2</sub>O<sub>2</sub>.** Up to three temperatures (30°C, 45°C—maximum operating temperature for the mercury vapor lamp—, and 60°C) and three concentrations of H<sub>2</sub>O<sub>2</sub> (14, 28, and 140 mmol L<sup>-1</sup>) were investigated. Results are depicted in Figures 5 and 6 for the standard and photo-activated oxidation, respectively.

**“Dark” Fenton.** Being an exothermic phenomenon, adsorption of paracetamol logically decreased with increasing

temperature (Figure 5A, B). If the initial rate of paracetamol oxidation was also improved by temperature, the effect on TOC reduction was less clear, resulting into an overall mineralization yield of about 30% for two times the stoichiometric amount of H<sub>2</sub>O<sub>2</sub> and 50% for a much larger oxidant excess in the whole temperature range (Figure 5C).

These effects can be better appreciated by examining H<sub>2</sub>O<sub>2</sub> consumption on Figure 5D. Regardless the initial amount of oxidant and the extent of TOC reduction, the oxidant was almost totally consumed at the highest temperatures. Therefore only a small fraction of H<sub>2</sub>O<sub>2</sub> was actually used to mineralize the pollutant and this efficient fraction (evaluated from Eq. 10) decreased from 18% to 5% when increasing oxidant concentration and temperature. It can be concluded that high temperature and large stoichiometric excess of oxidant are in fact useless.

**Photo-Fenton.** The same conclusion applied to photo-Fenton oxidation, where temperature and oxidant excess showed almost no effect on paracetamol conversion and mineralization, Figure 6. Full decomposition of peroxide was also achieved, but thanks to the promoting effect of UV/vis irradiation on radical production (Eqs. 3 and 4), the efficiency of consumed peroxide was greatly improved, especially at low oxidant concentration: up to 60% for a stoichiometric amount.

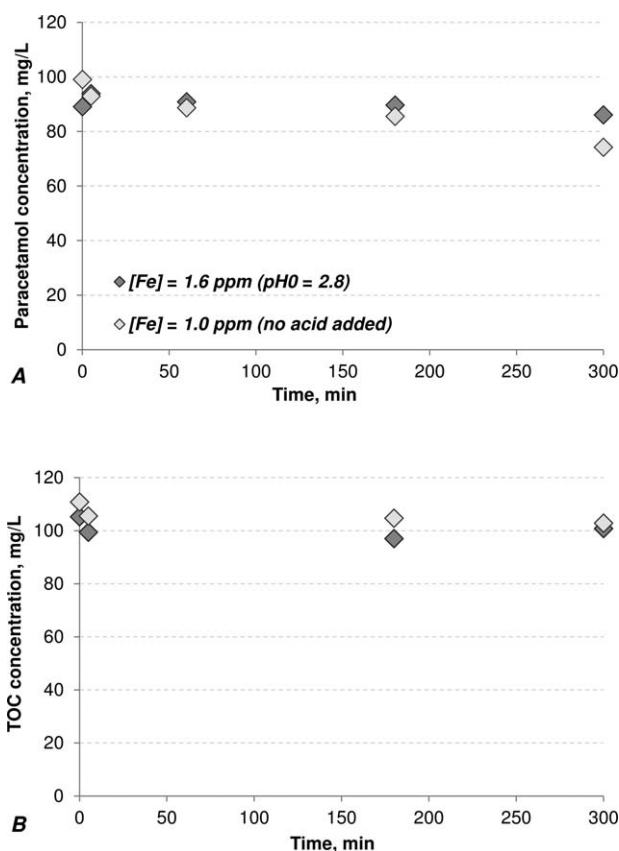


**Figure 7.** Catalytic activity of leachates from heterogeneous Fenton oxidation with 2 g L<sup>-1</sup> Fe/MFI: evolution of liquid phase concentrations of (A) paracetamol and (B) TOC.

Operating conditions:  $[P]_0 = 100 \text{ mg L}^{-1}$ ,  $[\text{H}_2\text{O}_2]_0 = 28 \text{ mmol L}^{-1}$ ,  $T = 60^\circ\text{C}$  (time zero corresponds to H<sub>2</sub>O<sub>2</sub> addition).

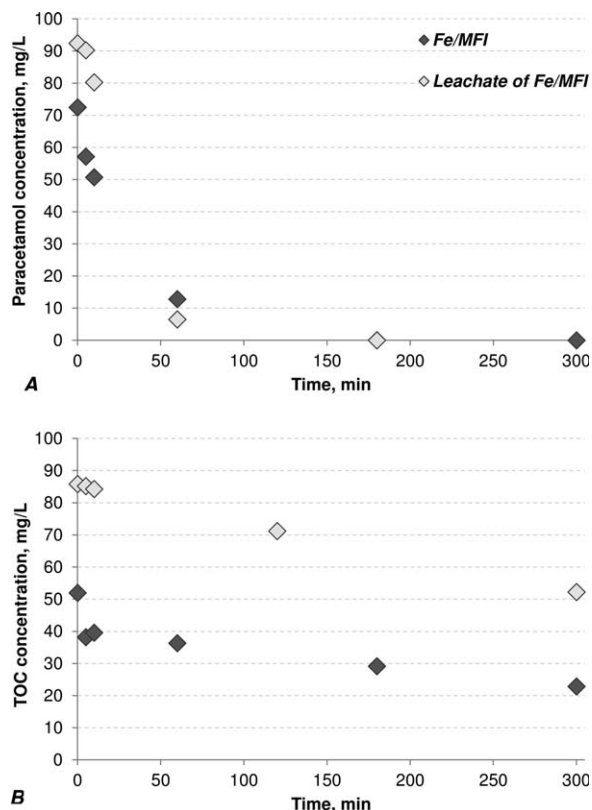


**Figure 8. Catalytic activity of Fe/MFI (2 g L<sup>-1</sup>) and corresponding leachate in photo-Fenton oxidation: evolution of liquid phase concentrations of (A) paracetamol and (B) TOC.**

Operating conditions: [P]<sub>0</sub> = 100 mg L<sup>-1</sup>, [H<sub>2</sub>O<sub>2</sub>]<sub>0</sub> = 14 mmol L<sup>-1</sup>, pH<sub>0,OX</sub> = 3.3–3.6, T = 30°C (time zero corresponds to H<sub>2</sub>O<sub>2</sub> addition).

### Mechanisms of “dark” Fenton and photo-Fenton oxidation using Fe/FMI

**Contribution of the Homogeneous Reaction.** Iron leaching is provoked by two mechanisms: “standard” dissolution by protons at low pH and promoted dissolution with the help of complexing agents, such as oxalic acid formed as oxidation

intermediate. Depending on whether it is complexed by water, hydroxyl or organic ligands, dissolved iron will exhibit a variable activity in “dark” Fenton and photo-Fenton oxidation, especially due to different quantum yields for the later.<sup>39</sup> To evaluate these effects, homogeneous oxidation tests were performed using leachates obtained after the heterogeneous reactions. The final suspensions were filtrated on a 0.2 μm pore-size membrane. Paracetamol and H<sub>2</sub>O<sub>2</sub> were added to the leachate so as to match the previous initial concentrations. Despite residual TOC in the solution, reaction was not therefore limited by the oxidant amount.

**“Dark” Fenton.** At 60°C and for a Fe/MFI concentration of 2 g L<sup>-1</sup>, leached iron varied in between 1.0 and 1.6 ppm (with preliminary acidification). The corresponding solubilized species did not show any significant activity in “dark” Fenton, Figure 7, either as the result of a too low concentration—the minimum recommended concentration of Fe<sup>2+</sup> or Fe<sup>3+</sup> for efficient Fenton oxidation<sup>40</sup> being in the range of 3 to 15 mg L<sup>-1</sup>—or because they formed stable ferric complexes with oxidation intermediates, impeding the Fe(II)/Fe(III) redox cycle.

**Photo-Fenton.** Similarly, a leachate recovered from a Fe/MFI suspension operated at 30°C was tested for UV/H<sub>2</sub>O<sub>2</sub> oxidation. In Figure 8, its activity is compared to that of the original suspension. Although the dissolved iron concentration was even lower than previously (0.36 mg L<sup>-1</sup>), it resulted here in a fast degradation rate of paracetamol and the mineralization yield was also high, 40% as compared to 58% for Fe/MFI under the same conditions. Photo-Fenton oxidation with Fe/MFI thus resulted from both homogeneous and heterogeneous mechanisms, the iron ferric complexes in solution being activated by the UV/vis irradiation.<sup>41</sup>

**Carbon Distribution.** To get a further insight of the oxidation mechanisms, values of residual carbon content in liquid and solid phases were compared on Figure 9 for all the investigated conditions. In most cases, carbon reduction was higher on the solid than in the liquid phase, probably as the result of a lower adsorption of the oxidation intermediates (especially carboxylic acids). Therefore based only on TOC concentrations in the liquid phase, mineralization yield would be underestimated by up to 12% (absolute error) at 2 g L<sup>-1</sup>.

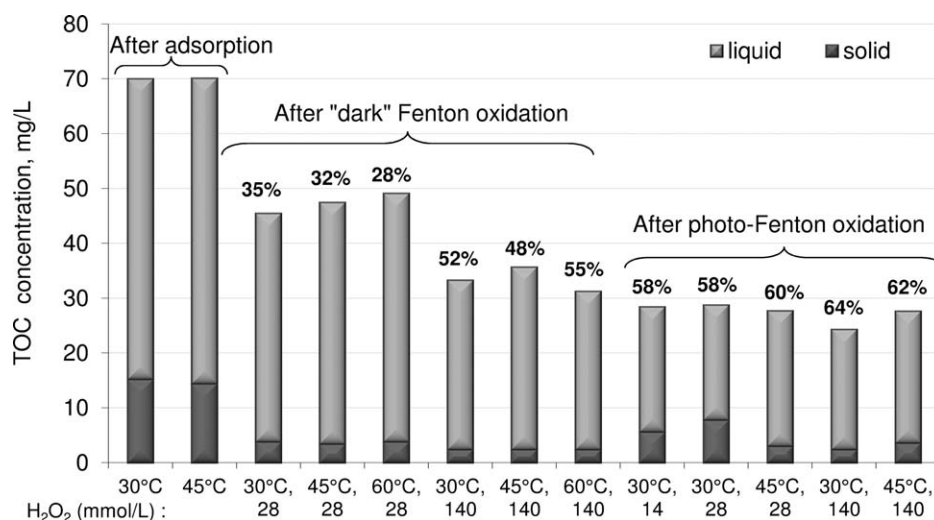


**Figure 9. Carbon speciation during “dark” Fenton and photo-Fenton oxidation catalyzed by Fe/MFI (values for solid phase have been converted in equivalent mg L<sup>-1</sup> of solution for comparison purpose).**

Overall mineralization yield is given above each bar. Operating conditions: [P]<sub>0</sub> = 100 mg L<sup>-1</sup>, [zeolite] = 2 g L<sup>-1</sup>.

**Table 2. Mineralization Yield After 5 h of Oxidation With 1 g L<sup>-1</sup> Maghemite (Sigma-Aldrich, S<sub>BET</sub> = 35.2 m<sup>2</sup>/g, d<sub>c</sub> (XRD) = 48 nm, d<sub>43</sub> = 4.8 μm) at pH<sub>0</sub> = 5.5 and in Brackets With 0.6 mmol L<sup>-1</sup> FeSO<sub>4</sub>·7H<sub>2</sub>O at pH<sub>0</sub> = 2.6: Operating Conditions: [P]<sub>0</sub> = 100 mg L<sup>-1</sup>**

Operating Conditions	Overall mineralization yield (%)
Fenton oxidation <sup>a</sup>	
[H <sub>2</sub> O <sub>2</sub> ] <sub>0</sub> = 14 mmol L <sup>-1</sup> , T = 45°C	18 (29)
[H <sub>2</sub> O <sub>2</sub> ] <sub>0</sub> = 153 mmol L <sup>-1</sup> , T = 60°C	9
Photo-Fenton oxidation	
[H <sub>2</sub> O <sub>2</sub> ] <sub>0</sub> = 14 mmol L <sup>-1</sup> , T = 45°C	42 (98)

<sup>a</sup>Leached iron: 0.1–0.2 ppm.

Despite a significantly better overall mineralization yield, the concentration of adsorbed carbon remained as high or even higher for photo-Fenton as compared to “dark” Fenton. It is consistent with a higher contribution of the homogeneous reaction under UV/vis irradiation. Other operating conditions (temperature, H<sub>2</sub>O<sub>2</sub> concentration) did not exhibit any clear effect on the carbon distribution.

**Comparison to Other Catalytic Systems.** In Velichkova et al.<sup>11</sup> the activity of different iron oxides was investigated for the Fenton oxidation of paracetamol in acidic pH conditions: hematite, maghemite, and magnetite. The last two being particularly active, they were further studied at the “natural” pH of the solution, leading to a maintained or even slightly improved performance of maghemite.<sup>42</sup> Table 2 shows the TOC abatement obtained with 1 g L<sup>-1</sup> of this iron oxide in different operating conditions. Assuming an iron density of 8.2 Fe atom/nm<sup>2</sup> for the main surface plane,<sup>43</sup> 1 g L<sup>-1</sup> of maghemite should correspond to about 0.5 mmol L<sup>-1</sup> of surface iron. Conversely, iron dispersion on Fe/MFI was measured at 22%, resulting in about 0.3 mmol L<sup>-1</sup> of available metal for 2 g L<sup>-1</sup> of this catalyst. Therefore the corresponding experiments should correspond to accessible iron concentrations of the same order of magnitude. Comparison of Table 2 with Figures 5 (Fenton) and 6 (photo-Fenton) shows a better performance of the iron supported zeolite, especially at high peroxide excess in dark conditions. This improved activity might result from the effect of zeolite as an adsorbing support, yielding a higher concentration of pollutant in the vicinity of the catalytic sites.

Table 2 also gives the results of the homogeneous system using 0.6 mmol L<sup>-1</sup> of Fe<sup>2+</sup> and 14 mmol L<sup>-1</sup> of H<sub>2</sub>O<sub>2</sub>: up to 98% mineralization was observed after 5 h of photo-activated oxidation, but not more than 30% in “dark” conditions. Note that for a much lower amount of dissolved iron (0.05 mmol L<sup>-1</sup>)—but still higher than that leached from Fe/MFI, Trovó et al.<sup>27</sup> achieved between 58% and 79% of TOC removal after 5 h of irradiation depending on the iron source (ferrioxalate or iron(II) sulfate). The authors used a starting H<sub>2</sub>O<sub>2</sub> concentration of 3.5 mmol L<sup>-1</sup> for 50 mg L<sup>-1</sup> of paracetamol and a new addition of peroxide (after 180 min) in the second case. The performance of Fe/MFI is therefore quite respectable compared to the homogeneous system, while eliminating the need for pH adjustment or post-treatment of the solution.

### Toward the development of a continuous process

**Catalyst Recycling.** The catalyst stability was first tested on recycling. The solid recovered after a “dark” Fenton oxidation (Fe/MFI 2 g L<sup>-1</sup>, 30°C, H<sub>2</sub>O<sub>2</sub> 28 mmol L<sup>-1</sup>) was washed several times with distilled water and dried at 70°C for 24 h.

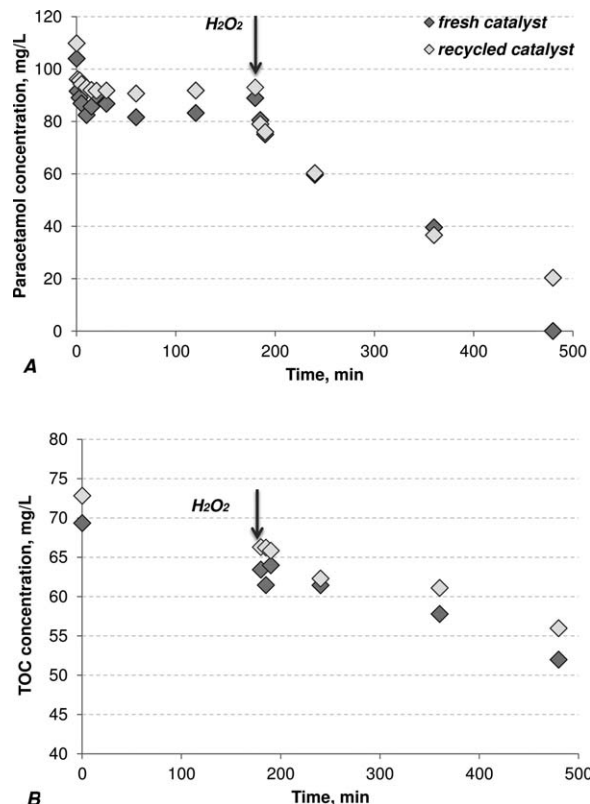


**Figure 10. Stability of Fe/MFI on recycling: evolution of liquid phase concentrations of (A) paracetamol and (B) TOC in solution during Fenton oxidation using fresh and recycled catalyst.**

Operating conditions: [P]<sub>0</sub> = 100 mg L<sup>-1</sup>, [zeolite] = 1 g L<sup>-1</sup>, [H<sub>2</sub>O<sub>2</sub>]<sub>0</sub> = 28 mmol L<sup>-1</sup>, T = 30°C.

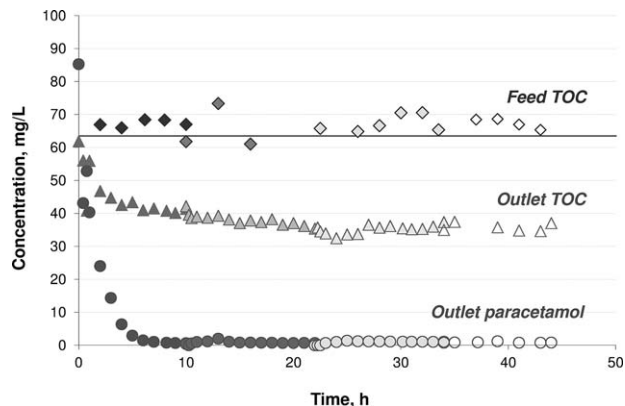
Due to inevitable loss, only a fraction was recycled and its activity was compared to that of the fresh catalyst at same concentration (1 g L<sup>-1</sup>).

Figure 10 shows a slight decrease in the adsorption capacity of the used zeolite from 17 to 15 mg g<sup>-1</sup> after 180 min of adsorption at 30°C, due to remaining adsorbed species from the initial experience. Oxidation then proceeded with almost the same rates with the used and fresh catalysts, whether regarding paracetamol degradation or TOC reduction in the liquid phase.

Table 3 confirms that the overall mineralization yield (including variations of carbon content on the solid phase) remained also unchanged, as well as the solution properties after zeolite contacting. The catalyst stability was further assessed using a continuous mode of operation.

**Table 3. Overall Mineralization Yield and Properties of the Solution Contacted with Fresh and Recycled Catalyst (Operating Conditions of Figure 10)**

Catalyst	Overall Mineralization Yield (%)	Fe in Solution (mg L <sup>-1</sup> )	pH After Adsorption	pH at the End of Oxidation
Fresh Fe/MFI	23	0.30	3.9 (±0.2)	3.2 (±0.2)
Recycled Fe/MFI	21	0.26	4.1 (±0.2)	3.1 (±0.2)



**Figure 11. Performance of a continuous system coupling photo-Fenton oxidation and microfiltration (for catalyst retention).**

Operating conditions:  $[P]_0 = 100 \text{ mg L}^{-1}$ ,  $[\text{zeolite}] = 2 \text{ g L}^{-1}$ ,  $[\text{H}_2\text{O}_2]_0 = 28 \text{ mmol L}^{-1}$ ,  $T = 30^\circ\text{C}$ ,  $Q_L = 0.2 \text{ L h}^{-1}$ ,  $V_L = 3 \text{ L}$  (photochemical + auxiliary reactors). Gray levels indicate different days of operation.

*Proof of Concept for the Continuous Process.* The continuous treatment test coupling photo-Fenton oxidation and membrane filtration (using an immersed microfiltration module) was lasted over 40 h. Steady state was reached after about 20 h, leading to a constant permeation flux and an almost unchanged TOC abatement of about 50% (see Figure 11). It is worth mentioning that according to Santos-Juanes Jordá et al.<sup>44</sup> this mineralization yield should significantly improve the biodegradability of the effluent: for the photo-Fenton oxidation of  $1 \text{ mmol L}^{-1}$  paracetamol solutions, bioassays with *P. putida* had shown a biodegradation efficiency over 90% when a 50% mineralization yield was achieved, compared to 30% with untreated paracetamol solution.<sup>44</sup>

Besides the effect of hydrodynamics (quasi CSTR behavior in the fast recycled loop reactors), the longer residence time (15 h vs. 5 h) required to reach the same TOC removal as in the corresponding batch experiment (58%, Figure 6B) might be explained by a much lower irradiated volume fraction (divided by 2).

The loss of iron in the purified water remained very low: less than 0.3 ppm, therefore below the EU requirement of 2 ppm.

## Conclusions

With more than 50% mineralization yield after 5 h in best conditions, Fe/MFI proved to be a convenient catalyst for photo-Fenton oxidation of paracetamol. Moreover it allowed to perform the reaction at natural pH and resulted in low iron leaching (below EU discharge standards). Nevertheless this low dissolved iron partly contributes to the clear positive effect of UV/vis irradiation. Conversely,  $\text{H}_2\text{O}_2$  concentration and temperature exhibited only a minor effect. In the  $0.5\text{--}2 \text{ g L}^{-1}$  range, an increase of the catalyst concentration improved the pollutant oxidation in “dark” conditions (no radical scavenging effect), but an optimum value was found under UV/vis irradiation due to the opposite effects of the increase in active sites and the photon absorption by the zeolite particles. Concerning the role of the zeolite support, it exhibited a significant adsorption capacity for the pollutant (about  $15 \text{ mg g}^{-1}$  in the investigated conditions) allowing its concentration close to the

catalytic sites, it afforded excellent iron dispersion and adequate surface acidity, but it had a limited effect on the pollutant oxidation otherwise due to its low capacity to decompose  $\text{H}_2\text{O}_2$ .

In a continuous process, the iron containing zeolite could be efficiently retained by a microfiltration membrane and showed almost constant activity over 40 h. Further work will study the application of this process to other pharmaceuticals.

## Acknowledgments

The authors are grateful to the French embassy in Sofia, the Working Community of the Pyrenees (CTP Project No. 11051939), Campus France and the Ministry of Education and Science of Bulgaria (PHC Rila No. 29619WF; D Rila 01/9-21.06.2013) for financial support. They also thank A. Tißler (Süd-Chemie AG, Clariant) for providing the zeolites, S. Adityosulindro, I. Benhamed, A. Ventas Gallego, O. Jacob Kjos-Hanssen (PhD and master students at LGC Toulouse), S. Desclaux (LGC, TOC), P. Jame (SCA-ISA, Lyon, carbon content), P. Mascunan (IRCELyon, CO chemisorption), J.F. Meunier (LCC, Mössbauer spectroscopy), M.L. Pern (SAP, LGC, HPLC/UV), G. Raimbeaux (SAP, LGC, porosimetry & TOC), C. Rey-Rouch (SAP, LGC, granulometry), D. Riboul (LGC, HPLC/MS), M.L. de Solan-Bethmale (SAP, LGC, ICP/AES), L. Vendier (LCC Toulouse, XRD) for their help on the catalyst and solution characterization, C. Albasi and P. Taillandier (LGC) for their advice on membrane selection, J.L. Labat and L. Farhi (LGC) for implementing the experimental setups.

## Literature Cited

- Mompelat S, Le Bot B, Thomas O. Occurrence and fate of pharmaceutical products and by-products, from resource to drinking water. *Environ Int.* 2009;35:803–814.
- Crane M, Watts C, Boucard T. Chronic aquatic environmental risks from exposure to human pharmaceuticals. *Sci Total Environ.* 2006; 367:23–41.
- Oller I, Malato S, Sánchez-Pérez JA. Combination of advanced oxidation processes and biological treatments for wastewater decontamination—a review. *Sci Total Environ.* 2011;409:4141–4166.
- Pignatello JJ, Oliveros E, MacKay A. Advanced oxidation processes for organic contaminant destruction based on the Fenton reaction and related chemistry. *Crit Rev Environ Sci Technol.* 2006;36:1–84.
- Minero C, Lucchiari M, Maurino V, Vione D. A quantitative assessment of the production of  $\cdot\text{OH}$  and additional oxidants in the dark Fenton reaction: Fenton degradation of aromatic amines. *RSC Adv.* 2013;3:26443–26450.
- Environmental Protection Agency. Parameters of water quality: interpretation and standards, Ireland; 2001:61–62. Available from: [https://www.epa.ie/pubs/advice/water/quality/Water\\_Quality.pdf](https://www.epa.ie/pubs/advice/water/quality/Water_Quality.pdf) (accessed Feb. 28, 2016).
- Hanna K, Kone T, Medjahdi G. Synthesis of the mixed oxides of iron and quartz and their catalytic activities for the Fenton-like oxidation. *Catal Commun.* 2008;9:955–959.
- Matta R, Hanna K, Chiron S. Oxidation of phenol by green rust and hydrogen peroxide at neutral pH. *Sep Purif Technol.* 2008;61:442–446.
- Hartmann M, Kullmann S, Keller H. Wastewater treatment with heterogeneous Fenton-type catalysts based on porous materials. *J Mater Chem.* 2010;20:9002–9017.
- Navalon S, Alvaro M, Garcia H. Heterogeneous Fenton catalysts based on clays, silicas and zeolites. *Appl Catal B.* 2010;99:1–26.
- Velichkova F, Julcour-Lebigue C, Koumanova B, Delmas H. Heterogeneous Fenton oxidation of paracetamol using iron oxide (nano)particles. *J Environ Chem Eng.* 2013;1:1214–1222.
- Yang XJ, Tian PF, Zhang XM, Yu X, Wu T, Xu J, Han YF. The generation of hydroxyl radicals by hydrogen peroxide decomposition on FeOCl/SBA-15 catalysts for phenol degradation. *AIChE J.* 2014; 61:166–176.

13. Minella M, Marchetti G, De Laurentiis E, Malandrino M, Maurino V, Minero C, Vione D, Hanna K. Photo-Fenton oxidation of phenol with magnetite as iron source. *Appl Catal B*. 2014;154–155:102–109.
14. Chen A, Ma X, Sun H. Decolorization of KN-R catalyzed by Fe-containing Y and ZSM-5 zeolites. *J Hazard Mater*. 2008;156:568–575.
15. Kasiri MB, Aleboye H, Aleboye A. Mineralization of C.I. Acid Red 14 azo dye by UV/Fe-ZSM5/H<sub>2</sub>O<sub>2</sub>, process. *Appl Catal B*. 2008;84:9–15.
16. Aleksić M, Kušić H, Koprivanac N, Leszczynska D, Božić AL. Heterogeneous Fenton type processes for the degradation of organic dye pollutant in water—the application of zeolite assisted AOPs. *Desalination*. 2010;257:22–29.
17. Duarte F, Madeira LM. Fenton- and photo-Fenton-like degradation of a textile dye by heterogeneous processes with Fe/ZSM-5 zeolite. *Sep Sci Technol*. 2010;45:1512–1520.
18. Gonzalez-Olmos R, Martin MJ, Georgi A, Kopinke FD, Oller I, Malato S. Fe-zeolites as heterogeneous catalysts for solar Fenton-like reactions at neutral pH. *Appl Catal B*. 2012;125:51–58.
19. Martucci A, Pasti L, Marchetti N, Cavazzini A, Dondi F, Alberti A. Adsorption of pharmaceuticals from aqueous solutions on synthetic zeolites. *Microporous Mesoporous Mater*. 2012;148:174–184.
20. Pasti L, Sarti E, Cavazzini A, Marchetti N, Dondi F, Martucci A. Factors affecting drug adsorption on beta zeolites. *J Sep Sci*. 2013;36:1604–1611.
21. Ternes TA. Occurrence of drugs in German sewage treatment plants and rivers. *Water Res*. 1998;32:3245–3260.
22. Kolpin DW, Furlong ET, Meyer MT, Thurman EM, Zaugg SD, Barber LB, Buxton HT. Pharmaceuticals, hormones, and other organic wastewater contaminants in U.S. streams, 1999–2000: a national reconnaissance. *Environ Sci Technol*. 2002;36:1202–1211.
23. Roberts PH, Thomas KV. The occurrence of selected pharmaceuticals in wastewater effluent and surface waters of the lower Tyne catchment. *Sci Total Environ*. 2006;356:143–153.
24. Rivera-Utrilla J, Sánchez-Polo M, Ferro-García MA, Prados-Joya G, Ocampo-Pérez R. Pharmaceuticals as emerging contaminants and their removal from water. A review. *Chemosphere*. 2013;93:1268–1287.
25. Durán A, Monteagudo JM, Carnicer A, Ruiz-Murillo M. Photo-Fenton mineralization of synthetic municipal wastewater effluent containing acetaminophen in a pilot plant. *Desalination*. 2011;270:124–129.
26. Almeida LC, Garcia-Segura S, Bocchi N, Brillas E. Solar photoelectro-Fenton degradation of paracetamol using a flow plant with a Pt/air-diffusion cell coupled with a compound parabolic collector: process optimization by response surface methodology. *Appl Catal B*. 2011;103:21–30.
27. Trovó AG, Pupo Nogueira RF, Agüera A, Fernandez-Alba AR, Malato S. Paracetamol degradation intermediates and toxicity during photo-Fenton treatment using different iron species. *Water Res*. 2012;46:5374–5380.
28. de Luna MDG, Briones RM, Su CC, Lu MC. Kinetics of acetaminophen degradation by Fenton oxidation in a fluidized-bed reactor. *Chemosphere*. 2013;90:1444–1448.
29. Cabrera Reina A, Santos-Juanes L, García Sánchez JL, Casas López JL, Maldonado Rubio MI, Li Puma G, Sánchez Pérez JA. Modelling the photo-Fenton oxidation of the pharmaceutical paracetamol in water including the effect of photon absorption (VRPA). *Appl Catal B*. 2015;166–167:295–301.
30. Yang L, Yu LE, Ray MB. Degradation of paracetamol in aqueous solutions by TiO<sub>2</sub> photocatalysis. *Water Res*. 2008;42:3480–3488.
31. Moctezuma M, Leyva E, Aguilar CA, Luna RA, Montalvo C. Photocatalytic degradation of paracetamol: intermediates and total reaction mechanism. *J Hazard Mater*. 2012;243:130–138.
32. Andreozzi R, Caprio V, Marotta R, Vogna D. Paracetamol oxidation from aqueous solutions by means of ozonation and H<sub>2</sub>O<sub>2</sub>/UV system. *Water Res*. 2013;37:993–1004.
33. Malato S, Fernández-Ibáñez P, Oller I, Prieto-Rodríguez L, Miralles-Cuevas S, Cabrera-Reina A. Approaches to water and wastewater treatment for removal of emerging contaminants: ongoing research and recommendations for future work (Chap. 5). In: Lambropoulou DA, Nollet LML. *Transformation Products of Emerging Contaminants in the Environment: Analysis, Processes, Occurrence, Effects and Risks*. Chichester: Wiley, 2014:161–178.
34. Haddou M. Dégradation de dérivés de l'acide benzoïque par les procédés d'oxydation avancée en phase homogène et hétérogène: procédé Fenton, photo-Fenton et photocatalyse, PhD Thesis, Université Toulouse III – Paul Sabatier, France; 2010. Available from: <http://thesesups.ups-tlse.fr/871/> (accessed Feb. 28, 2016).
35. Alvarez AM, Marchetti SG, Cagnoli MV, Bengoa JF, Mercader RC, Yeramian AA. Study of the Fe/Zelolite-L system Part II: CO and H<sub>2</sub> chemisorption behavior. *Appl Surf Sci*. 2000;165:100–108.
36. Park JY, Lee YJ, Khanna PK, Jun KW, Bae JW, Kim YH. Alumina-supported iron oxide nanoparticles as Fischer Tropsch catalysts: effect of particle size of iron oxide. *J Mol Catal A*. 2010;323:84–90.
37. Noh JS, Schwarz JA. Estimation of the point of zero charge of simple oxides by mass titration. *J Colloid Interf Sci*. 1989;130:157–164.
38. Fierro G, Moretti G, Ferraris G, Andreozzi GB. A Mössbauer and structural investigation of Fe-ZSM-5 catalysts: influence of Fe oxide nanoparticles size on the catalytic behaviour for the NO-SCR by C<sub>3</sub>H<sub>8</sub>. *Appl Catal B*. 2011;102:215–223.
39. Malato S, Maldonado MI, Fernández P, Oller I, Polo I. Decontamination of water by solar irradiation (Chap. 1). In: Litter MI, Candal RJ, Meichtry JM. *Advanced Oxidation Technologies: Sustainable Solutions for Environmental Treatments*. London: CRC Press Taylor and Francis Group, 2014:1–18.
40. Koprivanac N, Kušić H. AOP as an effective tool for the minimization of hazardous organic pollutants in colored wastewater; chemical and photochemical processes (Chap. 5). In: Lewinsky AA. *Hazardous Materials and Wastewater: Treatment, Removal and Analysis*. New York: Nova Science Publishers, 2007:149–199.
41. Rodriguez EM, Nunez B, Fernandez G, Beltran FJ. Effects of some carboxylic acids on the Fe(III)/UVA photocatalytic oxidation of muonic acid in water. *Appl Catal B*. 2009;89:214–222.
42. Velichkova F. Vers un procédé Fenton hétérogène pour le traitement en continu d'eau polluée par des polluants pharmaceutiques, PhD Thesis, INP Toulouse, France; 2014. Available from: <http://ethesis.inp-toulouse.fr/archive/00002806/01/velichkova.pdf> (accessed Feb. 28, 2016).
43. Daou TJ, Begin-Colin S, Grenche JM, Thomas F, Derory A, Bernhardt P, Legar P, Pourroy G. Phosphate adsorption properties of magnetite-based nanoparticles. *Chem Mater*. 2007;19:4494–4505.
44. Santos-Juanes Jordá L, Ballesteros Martín MM, Ortega Gómez E, Cabrera Reina A, Román Sánchez IM, Casas López JL, Sánchez Pérez JA. Economic evaluation of the photo-Fenton process. Mineralization level and reaction time: the keys for increasing plant efficiency. *J Hazard Mater*. 2011;186:1924–1929.